Advanced Steel Construction – Vol. 21 No. 2 (2025) 157–173
DOI:10.18057/IJASC.2025.21.2.7

TENSILE BEHAVIOR OF T-STUB TO HOLLOW SECTION COLUMN USING THREAD-FIXED ONE-SIDE BOLTS AT HIGH TEMPERATURES

Yang You [1, 2], Jing-Yu Wu [3, 4] and Bin Yang [5, *]

[1] *School of Transportation and Civil Engineering, Shandong Jiaotong University, China*
[2] *Shandong Key Laboratory of Technologies and Systems for Intelligent Construction Equipment, Shandong Jiaotong University, China*
[3] *Qingdao Geological Exploration Institute of China Metallurgical Geology Bureau, China*
[4] *School of Civil Engineering, Shandong University, Jinan, Shandong Province 256001, China*
[5] *Department of Civil and Environmental Engineering, The Hong Kong Polytechnic University, Hong Kong, China*
** (Corresponding author: E-mail: bin24.yang@connect.polyu.hk)*

ABSTRACT

The Thread-fixed One-side Bolt (TOB), which utilizes internal threads in the bolt hole instead of a nut, enables installation from one side, thereby overcoming the challenge of connecting closed-section components, such as steel tube columns, which are not suitable for traditional bolt connections. This study establishes and validates a Finite Element Model (FEM) to investigate the mechanical performance of TOB connections under high temperature conditions. The results show that the wall thickness of the column has a significant influence on the performance of the connection; an increase in wall thickness substantially enhances both stiffness and bearing capacity. For columns with thinner walls, applying preload can improve stiffness. Furthermore, increasing the material strength of the column wall improves bearing capacity but has little effect on stiffness. For columns with insufficient wall thickness, the mechanical performance of the connection can be significantly enhanced by installing Internal Constraint Components (ICC) within the tube. Based on the FEM analysis results, a calculation method for the bearing capacity of TOB connections, accounting for high-temperature deformation and material degradation, is proposed. This method accurately predicts the yield bearing capacity at different temperatures. This research provides theoretical support for the design and application of TOB connections in engineering.

ARTICLE HISTORY

Received: 7 July 2024
Revised: 25 December 2024
Accepted: 1 January 2025

KEYWORDS

One-side bolt;
High temperature;
Tensile behavior;
Closed section

1. Introduction

The blind bolt, or one-side bolt, is a type of fastening system designed to provide a bolting option for structures where access is only available from one side. This situation is common in construction and manufacturing industries where it is either impossible or impractical to access both sides of the structure being connected, such as closed steel sections. The development of blind bolts arose from the need for an effective fastening solution in situations where Traditional Bolts (TB) were not feasible. TB require access to both sides of the structure for installation: one side to insert the bolt and the other side to secure the nut. In many modern construction and manufacturing scenarios, such as in hollow steel structures or areas with restricted access, this two-sided access is not possible. Blind bolts were developed to address this limitation, offering a reliable and robust fastening solution that can be installed from one side only [1].

Before the advent of blind bolts, the installation of closed-section steel components such as steel tube columns could only be completed through welding. Welded connections in steel structures offer strong and continuous connections but have notable disadvantages. They require skilled labor and precision, making the process costly due to the need for specialized equipment and rigorous inspections, including X-ray or ultrasonic testing. Welds can be prone to brittle fractures, especially in high-strength steels and under adverse conditions like low temperatures or high-impact loads. The welding process can introduce residual stresses and deformations in steel members, potentially compromising structural integrity. Additionally, welded connections may have lower fatigue strength and are more susceptible to corrosion. On-site welding presents challenges due to environmental factors, affecting weld quality. Repairs or modifications in welded structures can be cumbersome, often necessitating extensive cutting and re-welding.

Due to the various disadvantages of welding connections, the emergence of blind bolts immediately attracted widespread attention. Many researchers began to study the mechanical properties of blind bolts. Currently, the most researched is the Hollo Bolt [2]. During installation, the bolt is inserted into a pre-drilled hole, and then the bolt is tightened, which activates the expansion mechanism on the blind side, completing the connection. Wang et al. [3] investigated the tensile performance of connections using Hollo Bolt through experiments and the numerical simulation. Their experiments used T-stub connections and they established design equations for the stiffness and load-bearing capacity of such T-stub connections using Hollo Bolt. Cabrera [4] studied the pre-tension force of Extended Hollo-Bolts. The results showed that the special anchoring mechanism of this type of bolt leads to a pre-tension force coefficient much larger than that of TB. If conventional bolt pre-tension coefficients are used to apply torque to these bolts, it may result in excessive pre-tension forces. Pan et al. [5] conducted experimental research on the low-cycle fatigue performance of Hollo Bolt-connected T-stub connections. Based on the experimental results, they analyzed the typical failure modes, strength degradation, and energy dissipation of the connections. Furthermore, they proposed an energy-based damage model and equations for calculating fatigue life. Pascual et al. [6][7] studied the fire response of Square Hollow Section (SHS) column connections using Hollo bolt, finding that size of the column section and bolt type have a minor impact on the fire behavior. However, the presence of concrete significantly slows the temperature increase rate. Song [8] found that applying fire protection measures to steel beams or reducing the load ratio of steel beams can effectively enhance the fire resistance of Hollo Bolt connection. However, placing binding bars in the connection or changing the material of columns has a limited impact on the fire performance of Hollo Bolt connections. However, the structure of the Hollo Bolt itself is complex, which leads to greater manufacturing difficulty and a cost that can be more than ten times higher than that of traditional bolts. Additionally, the bolt relies on the deformation of the outer sleeve to provide anchorage, and once installed, it is difficult to remove, which is unfavorable for later maintenance. As a result, the use of Hollo Bolt is somewhat limited.

In addition to the Hollo Bolt, there are other methods for achieving one-sided bolt installation. The Ajax ONESIDE bolt features a special foldable washer that can pass through the bolt hole when folded. Once inserted, a special tool allows the washer to unfold on the blind side, completing the anchorage. Lee et al. [9] found that the Ajax ONESIDE bolt connection in T-stub to hollow steel tube column connections meets the requirements for semi-rigid connections. Research by Hosseini [10] shows that Ajax ONESIDE bolt connections perform satisfactorily under monotonic and repeated shear forces, meeting the demand in EN 1993-1-8 [11] for bolted connections. Similarly, one-side anchoring can be achieved by incorporating a rotatable pin on the bolt shank, which, after passing through the bolt hole, rotates perpendicular to the hole for anchorage. Alternatively, both the nut and bolt hole can be made elliptical, with the nut slightly smaller. The nut passes through the bolt hole when aligned parallel, and the bolt is then rotated to change the orientation from parallel to perpendicular for blind-side anchoring. Wan [12] and Sun [13] found that the aspect ratio of the bolt head has minimal impact on the yield load capacity of the connection. An aspect ratio of 1.7 for the bolt head balances bolt slippage and stress concentratio7n around the bolt hole, achieving the most advantageous connection.

Although the aforementioned blind bolts enable one-side installation, their performance is not satisfactory enough. For example, the load-bearing capacity of Ajax ONESIDE bolts depends on the strength of the folded washer, and the

strength of the bolt shaft itself is difficult to fully utilize, making it hard to achieve the same performance as traditional high-strength bolts. Attaching a rotatable pin to the bolt shank weakens the cross-section of the bolt, affecting both its tensile and shear load-bearing capacities. Using bolts with elliptical nuts and bolt holes also affects the shear capacity along the long axis of the bolt hole. Li et al. [14] conducted experiments comparing the connection performance of different types of blind bolts and traditional bolts. The results showed that the strength and stiffness of joints connected with existing blind bolts were less than half of those using traditional bolts (TB). As a result, many researchers are continuously working on improving the blind bolts to achieve better mechanical performance [15]-[19]. By directly setting threads inside the bolt hole, nuts can be replaced to anchor bolts for one-side installation, known as Thread-fixed One-side Bolts (TOB). TOB is structurally simple and convenient for installation, allowing the use of standard bolts and tools. This type of connection has been widely used in bolt-ball joints and some mechanical structures. However, as the wall thickness and strength of typical steel tube columns are generally less than nuts, the effectiveness of TOB connections needs verification. You [19][20] and Wang [21] conducted experiments on TOB connections and found that bolt pull-out failure does not occur even with limited wall thickness before overall connection yielding. However, the limited number of experimental specimens presents challenges in establishing and fully validating precise load-bearing capacity equations. Additionally, it is difficult to observe the deformation process of connections and the stress-strain distribution within the threaded holes, particularly the yield line distribution on the surface of steel tube columns without nut constraints, through experimental methods. Furthermore, the influence of key parameters such as bolt pre-tension, material strength, and elevated temperatures warrants further investigation.

Based on existing experiments, this paper establishes and validates a Finite Element Model (FEM) to study the mechanical performance of TOB bolted connections at elevated temperatures. The main failure modes of the connections and the causes of failure are analyzed, and the degradation patterns of the load-bearing capacity and stiffness of the connection at high temperatures are discussed. Additionally, based on the FEM analysis results, a method for calculating the load-bearing capacity of TOB bolted connections at different temperatures is proposed and discussed.

2. Finite element model

2.1. Establishment of the model

To accurately simulate the mechanical performance of TOB bolted connections under varying temperatures, it is essential to account for factors such as material nonlinearity under the combined effects of thermal and force fields, nonlinear contact relationships between different parts, and geometric nonlinearity. Additionally, while analyzing the overall macroscopic performance, the performance of microscopic components, such as the threads inside the bolt hole and on the bolt shank, must also be considered. Therefore, establishing the model is highly complex and requires certain simplifications.

To reduce computational difficulty and improve efficiency, this paper focuses on analyzing the tensile area of TOB bolted connections in the model. Following the component method, a connection can be divided into several simple components. Using the component method, a connection can be divided into several simple components. Analyzing these components separately and then combining them can represent the overall behavior of the connection. According to P398 [22], the bolted beam-column end-plate connections can be divided into different parts such as tensile area, compression area, vertical shear area, and horizontal shear areas. From the perspective of load transfer mechanism, TOB and TB differ only under tensile forces. Therefore, in this paper, only the tensile area of the beam-column end-plate connection was selected for analysis to reduce computational complexity, as shown in Fig. 1.

Considering the symmetry of the tensile zone, only a 1/8 model was established for analysis. Corresponding boundary conditions were applied on the symmetry planes, as shown in Fig. 2. The load on the connection was applied in the form of displacement. In the model, all components used hexahedral linear reduced integration elements C3D8R. The model was meshed with cubic grids of 0.3mm edge length, with local refinement at critical areas such as the threads inside the bolt hole and on the bolt shank.

High-strength steel and ordinary structural steel exhibit different reduction speeds at high temperatures due to variations in composition and processing, as shown in Fig. 3. Ignoring these differences may lead to inaccurate simulation results. Therefore, in the FEM of this paper, different constitutive relationships were used for ordinary structural steel and bolts. Ordinary structural steel followed the stress-strain relationship model and high-temperature reduction factors recommended by EN 1993-1-2 [24], while the bolts were modeled based on experimental data from Pang et al [25]. The constitutive relationship models for ordinary structural steel and bolts in the FEM are shown in Fig. 4.

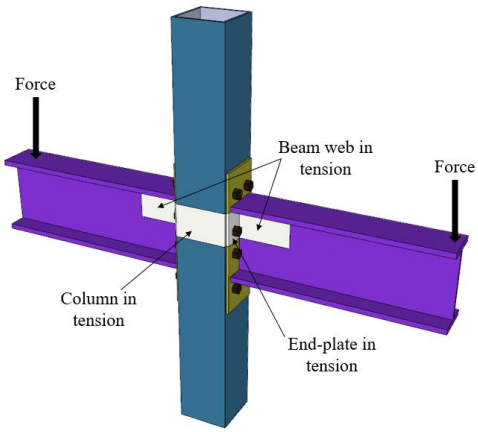

Fig. 1 The Tension zone of a bolted end-plate connection

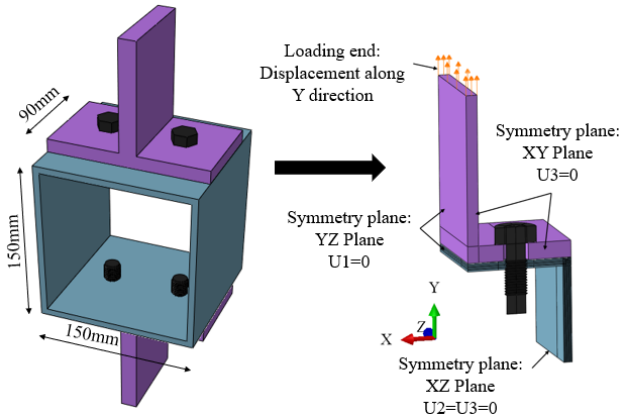

Fig. 2 The boundary conditions and loads of the FEM

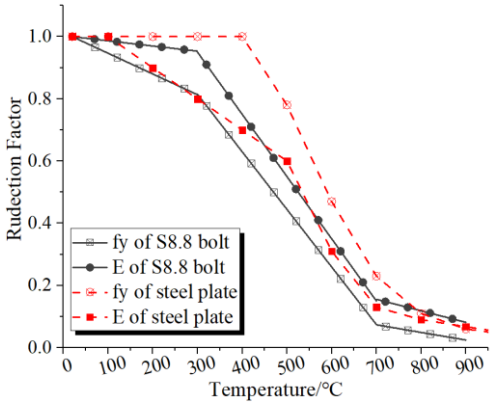

Fig. 3 Comparison of the reduction factor of mild steel and high strength bolt[24][25]

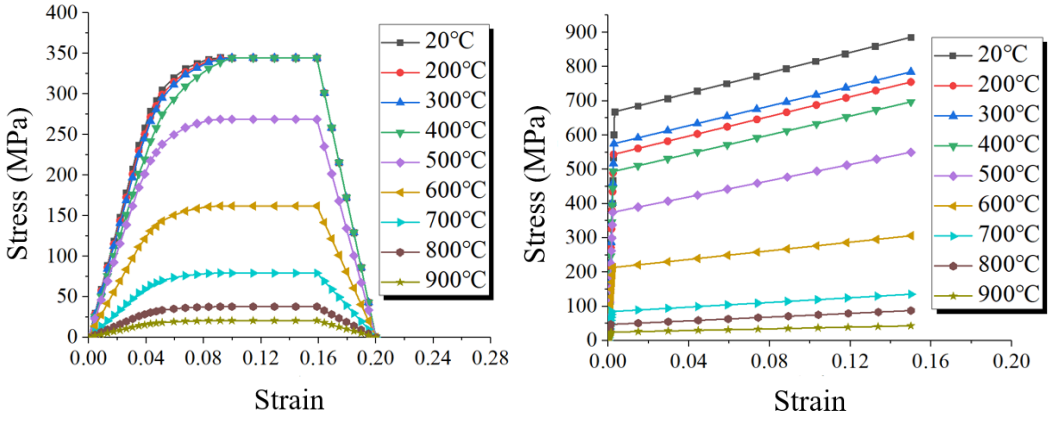

(a) mild steel (Q350) (b) bolt

Fig. 4 The consecutive law of mild steel and bolt applied in FEM.

In finite element modeling analysis, such as using Abaqus software, it is necessary to convert nominal stress-strain data to true stress-strain data. This is because true stress-strain more accurately reflects the material's real mechanical behavior during the plastic deformation process. Nominal stress-strain is defined based on the initial cross-sectional area and length of the specimen, assuming these parameters remain constant during deformation. However, in reality, the cross-sectional area changes significantly as deformation occurs, especially in the large plastic deformation stage. In contrast, true stress-strain considers the instantaneous cross-sectional area and cumulative deformation effects, providing a more precise description of the material's mechanical response. This true stress-strain relationship not only better meets the requirements of material models in finite element analysis but also avoids computational errors caused by the limitations of engineering stress-strain under large deformation conditions. Therefore, Equations (1), (2), and (3) were used in the FEM to convert nominal stress σ_{nom} and nominal strain ε_{nom} into true stress σ_{true} and true strain ε_{true}, respectively.

$$\varepsilon_{true} = \ln(1+\varepsilon_{nom}) \tag{1}$$

$$\sigma_{true} = \sigma_{nom}(1+\varepsilon_{nom}) \tag{2}$$

$$\varepsilon_{pl} = \varepsilon_{true} - \frac{\sigma_{true}}{\varepsilon} - \varepsilon_{thermal} \tag{3}$$

In terms of contact relationships, the model employs a general contact approach where the normal direction is set to hard contact, and the tangential contact is defined using the Coulomb friction model. Referring to the Chinese code GB50017-2017 [26] and other relevant studies [27]-[32], the FEM in this paper assumes a friction coefficient of 0.3 for tangential contact.

The model includes initial step and two analysis steps. The initial step is set to define the boundary conditions and the thermal field. The first analysis step is used to apply the preload of bolt, while the second analysis step involves the application of displacement load.

2.2. Validation of the model

To verify the accuracy of the model calculations, three sets of test specimens were designed and tested at both room and high temperatures. These tests provided a basis for validating the FEM model's accuracy. The test specimens included two T-stubs and a steel tube, connected by four bolts. The bolt holes on the surface of the steel tube were threaded to provide anchorage for the TOB. The bolt holes on the T-stub were plain holes, 2mm larger than the TOB. Other relevant information can be found in Fig. 5 and Table 1. The bolts used were standard grade 8.8 high-strength bolts, with thread dimensions conforming to Chinese standards GB/T 192-2003 [33] and GB/T 192–-2003 [34].

The test was conducted using a universal testing machine with a load capacity of 1000 kN and an accompanying electric furnace, as shown in Fig. 6. Prior to loading, the bolts were pre-tensioned according to the requirements in GB 50017-2017 [26]. The assembled specimens were then installed on the testing machine for preloading. The main steps of preloading involved loading the specimen from 0 kN to 10 kN, then unloading back to 0 kN while keeping the grips of the testing machine tight. This preloading process helps to reduce potential slippage and deformation during the actual test, ensuring accurate loading and measurement.

Table 1
Test specimens

	Column wall thickness t_c/mm	T-stub flange thickness t_c/mm	H-section steel flange thickness t_c/mm	Bolt diameter D/mm
S1	6	12		16
S2	12	12		16
S3	6	12	6	16

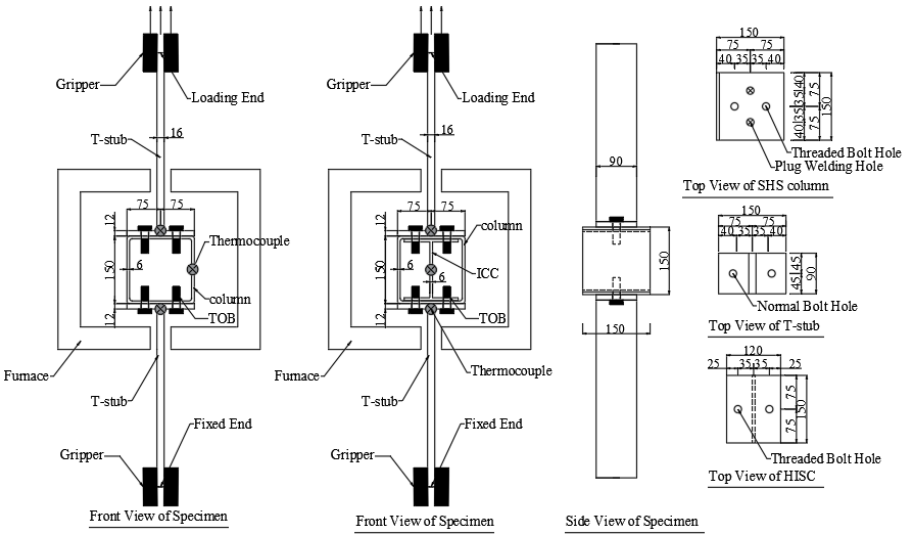

Fig. 5 Test specimen

After preloading, the specimens were loaded to failure at a rate of 2 mm/min. During loading, the deformation and load were automatically recorded by the control computer of the testing machine. Dial gauges were also installed to measure the deformation of the test specimens, verifying the data recorded by the testing machine. This ensured the accuracy and reliability of the measurement results.

The high-temperature test was conducted using steady-state method. The specimens were first heated to the specified temperature and maintained for 30 minutes, with one end clamped and the other free to prevent additional stress from temperature changes. Preloading was then performed. After completing the preloading, the specimens were loaded to failure at a rate of 2 mm/min. The preloading process and data measurement methods were the same as those used in the room temperature tests. Before the tests, corresponding steel samples were retained and processed into standard specimens to test their material properties. The actual measured material properties were used for modeling and verification.

The load-displacement curves of TOB bolted connections show apparent non-linear characteristics after the initial elastic stage and lack a distinct yield plateau, making it difficult to directly determine the yield bearing capacity (F_Y). By employing the tangent method, the yield bearing capacity F_Y of the connections at different temperatures can be determined [35]-[37]. Additionally, the ultimate bearing capacity (F_U) of the connections can be obtained from the highest point of the curves, as shown in Fig. 7

Fig. 8 compares the FEM and experimental results of the S1 group. The steel tube in the S1 group had a wall thickness of only 6mm. As the load increased, the walls of the steel tube deformed. The two side walls deformed inward, while the top and bottom surfaces deformed outward. Due to the deformation of the steel tube, disengagement occurred between the threaded hole and the TOB, resulting in a nonuniform stress and strain distribution inside the threaded hole. This nonuniformity ultimately resulted in the pullout of the TOB and the failure of the connection. The phenomena observed in the simulation were consistent with those observed in the test.

The S2 group specimens initially formed a plastic zone at the intersection of the web and flange of the T-stub. Subsequently, the deformation rapidly increased, leading to significant deformation of the bolt. However, only discontinuous and minor plastic strain accumulation occurred in the threads inside the bolt hole, indicating no damage to the threads within the bolt hole.

Fig. 6 Test setup

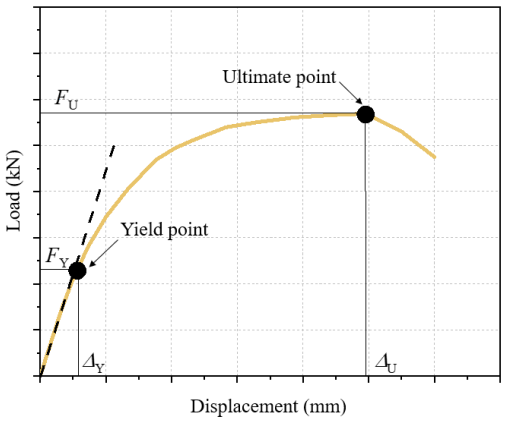

Fig. 7 Load-displacement curve

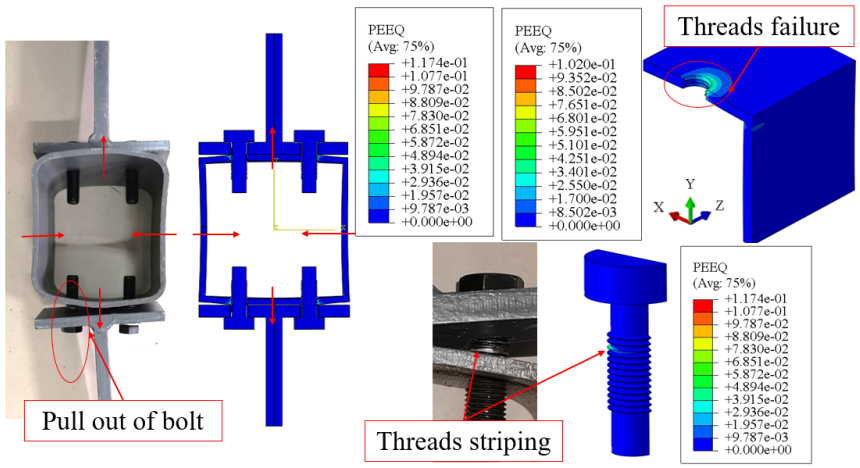

(a) Comparison of S1 group

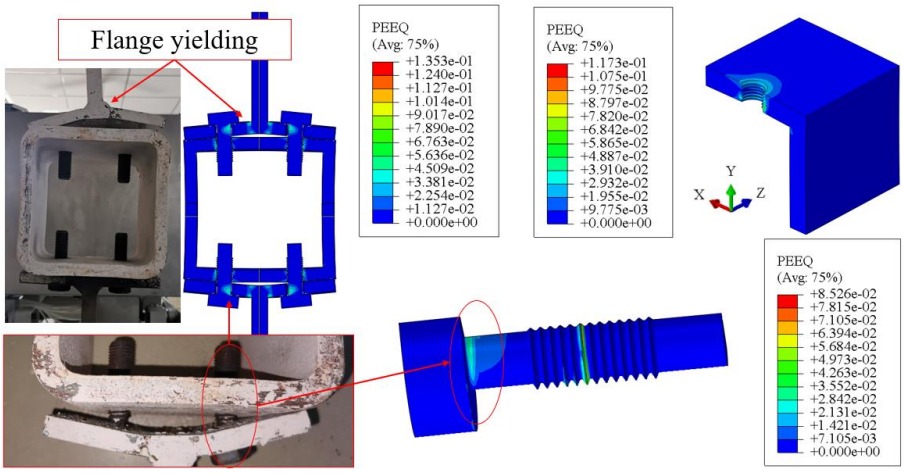

(b) Comparison of S2 group

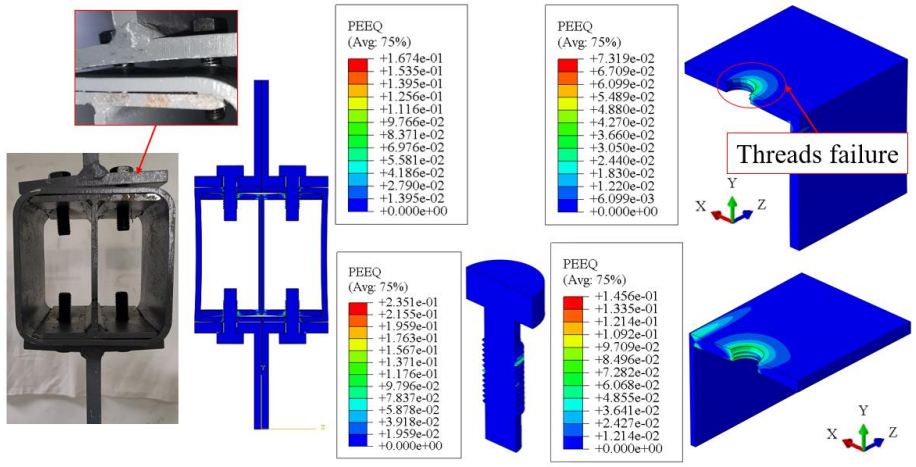

(c) Comparison of S3 group

Fig. 8 Comparison of simulation result and test result

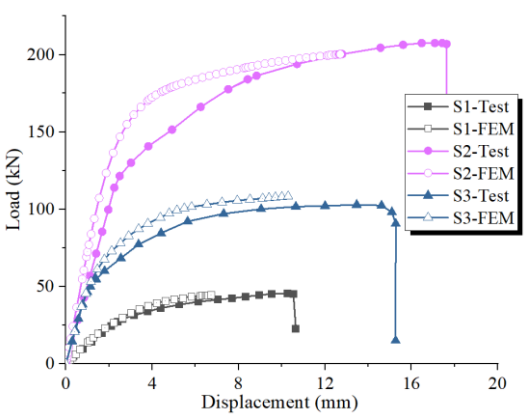

(a) Comparison of load-displacement curves at 20℃

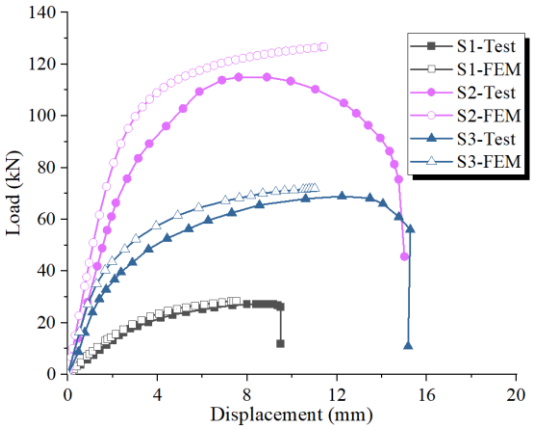

(b) Comparison of load-displacement curves at 500℃

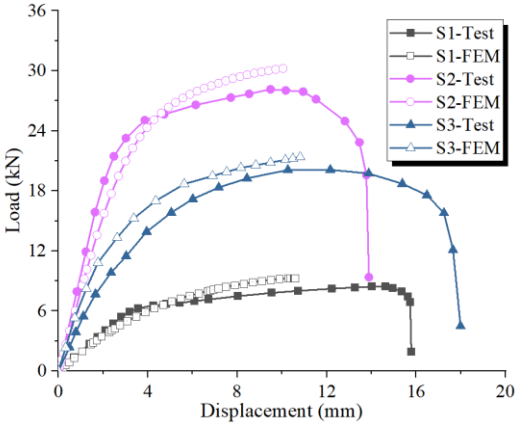

(c) Comparison of load-displacement curves at 700℃

Fig. 9 Comparison of simulation result and test result

For the S3 group specimens, the overall deformation of the connection was small, but significant plastic strain was observed in the threads of the bolt holes in both the steel tube column and the infilled H-section steel, consistent with the bolt pullout phenomenon observed in the test.The simulation results for each group of specimens were consistent with the phenomena observed in the tests.

Fig. 9 compares the load-displacement curves of different specimens. Compared to the S1 group, both the S2 and S3 groups show significant improvements in yield load capacity F_Y, ultimate load capacity F_U, deformation capacity, and stiffness at the same temperature. For instance, at room temperature, the yield load capacity F_Y and ultimate load capacity F_U of the S2 group are approximately 4.2 times and 4.1 times those of the S1 group, respectively. This improvement is primarily attributed to the change in the anchorage capacity of the threaded hole. The failure mode of the S1 group specimens is tube column wall yielding, which leads to the separation of the threaded hole and TOB when the column wall deforms. As a result, the connection fails quickly after yielding. In contrast, for the S2 and S3 groups, after yielding, the separation between the TOB and the threaded hole does not occur immediately, allowing for further increase in the load-bearing capacity after connection yielding.

It should be noted, however, that although both the S2 and S3 groups have a bolt anchorage depth of 12 mm, the load-displacement curves of the two groups exhibit significant differences. Under the same temperature, the initial stiffness, yield load capacity F_Y, and ultimate load capacity F_U of the S2 group are all higher than those of the S3 group. Specifically, at the same temperature, the yield load capacity F_Y and ultimate load capacity F_U of the S2 group are approximately 2.5 times and 2.1 times those of the S3 group, respectively, as shown in Table 2. This difference arises because the Internal Constraint Components and the steel tube column wall work separately, with only minimal interaction between them. This suggests that directly increasing the thickness of the steel tube wall is more efficient than installing Internal Constraint Components.

The comparison in Fig. 9 shows that the load-displacement curves obtained from finite element calculations closely match those from test results. Table 2 shows that the relative error between the model's output of the yielding load (F_Y) and ultimate load (F_U) and the experimentally obtained load capacity increases with the rise in temperature (θ), but remains within the range of -8.1% to 16.8%. Overall, the finite element model established in this paper can accurately reflect the failure characteristics of TOB connections at different temperatures. Additionally, the model's load-displacement curves and load capacities are consistent with test results, demonstrating good accuracy.

Table 2
Comparison of test result and simulation result

	Temperature θ (℃)	Test			FEM			Error (FEM - Test) / Test	
		Failure mode	Yielding load F_Y (kN)	Ultimate load F_U (kN)	Failure mode	Yielding load F_Y (kN)	Ultimate load F_U (kN)	Yielding load F_Y (kN)	Ultimate load F_U (kN)
S1	20	mode1	28.1	41.9	mode1	27.8	44.5	-1.1%	6.2%
	500	mode1	17.2	27.2	mode1	15.8	28.5	-8.1%	4.8%
	700	mode1	5.5	7.5	mode1	6.2	8.2	12.7%	9.3%
S2	20	mode2	118.8	173.4	mode2	113.4	180.3	-4.5%	4.0%
	500	mode2	68.5	113.2	mode2	68.8	112.7	0.4%	-0.4%
	700	mode2	17.5	25.9	mode2	19.2	29.1	9.7%	12.4%
S3	20	mode1	45.2	82.1	mode1	47.1	77.5	4.2%	-5.6%
	500	mode1	26.2	48.5	mode1	26.1	48.4	-0.4%	-0.2%
	700	mode1	7.2	13.1	mode1	7.5	15.3	4.2%	16.8%

3. Parameter analyzes and discussion

3.1. Influence of tube wall thickness

Based on the parameters of the connection, including the bolt diameter D, steel tube wall thickness t_c, and T-stub thickness t_T, four potential failure modes for TOB connections are identified: tube column wall yielding (mode 1), T-stub flange yielding accompanied by bolt failure (mode2), T-stub flange yielding (mode3), and bolt fracture failure (mode4). Notably, failure mode 1 results in a failure mechanism for TOB connections that differs significantly from that of TB connections. This is due to the absence of deformation restraint from the nut on the steel tube column wall and the lack of anchorage provided by the nut. In contrast, other failure modes do not involve damage to the steel tube column or the threaded hole, resulting in no significant difference in the failure mechanism between TOB and TB connections. Given the multiple potential failure modes of the TOB connection, this paper focuses its analysis primarily on failure mode 1 for convenience.

For TOB connections, the steel tube wall thickness (t_c) determines the anchoring depth that the threaded hole can provide. Additionally, the wall thickness (t_c) also influences the deformation capability of the steel tube, which in turn affects the contact relationship between the threaded hole and the TOB. Therefore, the steel tube wall thickness (t_c) is one of the most crucial parameters influencing the behavior of TOB connections. Using the verified FEM, the failure mechanisms of TOB connections with different steel tube wall thicknesses (t_c) and their reduction under high temperatures were analyzed. During the analysis, the bolt diameter (D) of the selected connections was consistently 16mm, and the steel tube section width (b_c) was 150mm. The analysis of the model is limited to temperatures below 800°C. This is because, after exceeding 500°C, the material properties of steel, including elastic modulus, yield strength, and ultimate strength, undergo a significant degradation. At temperatures of 800°C or higher, steel essentially loses its load-bearing capacity. According to the data provided in the European standard EN1993-1-2, at 800°C, the yield strength of ordinary steel is only 11% of its value at room temperature, and the elastic modulus is only 9% of its room temperature value. Therefore, before reaching 800°C, the connection will have already failed under the action of sustained loads, making further discussion of conditions at or above 800°C unnecessary.

At the same temperature θ, as the tube wall thickness (t_C) increases, the failure mode of the connection gradually changes from tube column wall yielding (mode 1) to T-stub flange yielding accompanied by bolt failure (mode 2). Fig. 10 and Fig. 11 show the stress and strain distribution in the threads inside the bolt hole for the connection with 6mm t_C (mode 1) and 12mm t_C (mode 2), respectively, at different temperatures θ when reaching the yield load (F_Y).

For connection with 6mm t_C, when reaching the yield bearing capacity F_Y, the stress distribution inside the threaded hole is nonuniform due to the deformation of the steel tube. The plastic equivalent strain PEEQ mainly occurs on the side with higher stress, as shown in Fig. 10 (a). With the increase in temperature, the deformation of the connection increases, leading to even more uniform stress and strain distribution inside the threaded hole, as depicted in Fig. 10 (b). This nonuniform stress distribution caused by column wall deformation leads to the failure of the connection.

For connection with 12mm t_C, the greater stiffness of the tube means that, upon reaching the yield bearing capacity F_Y, the deformation mainly occurs in the flange of the T-stub. The stress distribution in the threads inside the bolt hole is uniform, and the plastic strain predominantly occurs at the root of the threads in the lower part, while the upper threads remain elastic. This indicates that the threads inside the hole can provide sufficient anchorage for the bolt, as shown in Fig. 11.

Fig. 12 (a) indicates that the initial stiffness K of the connection rapidly increases with the increase in tube wall thickness t_C. However, when the fire temperature θ exceeds 500°C, a significant decrease in the initial stiffness K is observed. The influence of tube wall thickness t_C on the initial stiffness K becomes substantially less significant. At temperatures θ exceeding 700°C, the connections almost completely lose their load-bearing capacity, and the effect of variations in t_C on the initial stiffness K becomes negligible.

Similarly, when the fire temperature θ does not exceed 500°C, increasing in t_C can significantly improve the yield load F_Y and ultimate load F_U. However, as the temperature θ exceeds 500°C, the load-bearing capacity of the connection substantially decreases, and the influence of steel tube wall thickness t_C on the load-bearing capacity reduces. When the temperature θ exceeds 700°C, the influence of tube wall thickness t_C on the load-bearing capacity of the connection becomes minimal.

Fig. 12 (b) and (c) shows that the reduction factors of tensile load at the same temperature are not significantly different, and the failure mode does not change with variations in temperature. This indicates that the mechanical performance of TOB connection is stable under different temperatures.

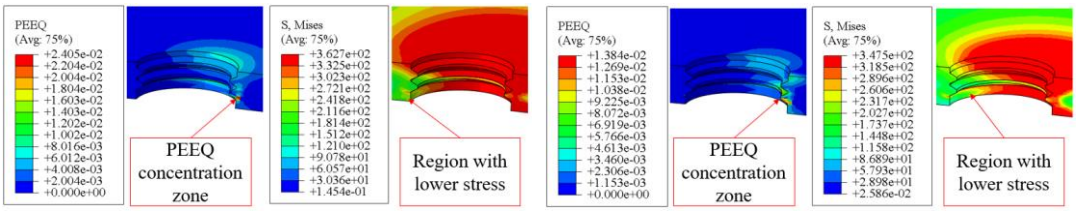

(a) θ=20℃ (b) θ=500℃

Fig. 10 The state of the hole threads under yielding load F_Y (t_C=6mm)

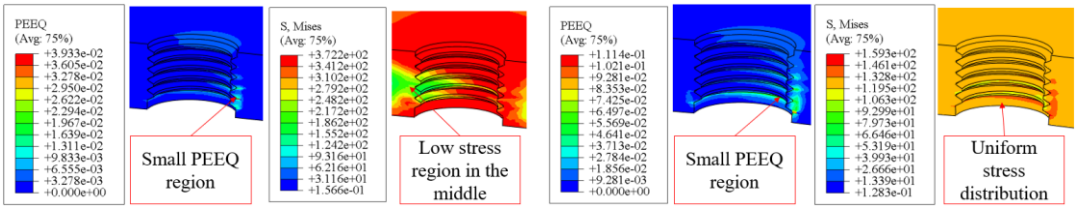

(a) θ=20℃ (b) θ=500℃

Fig. 11 The state of the hole threads under yielding load F_Y (t_C=12mm)

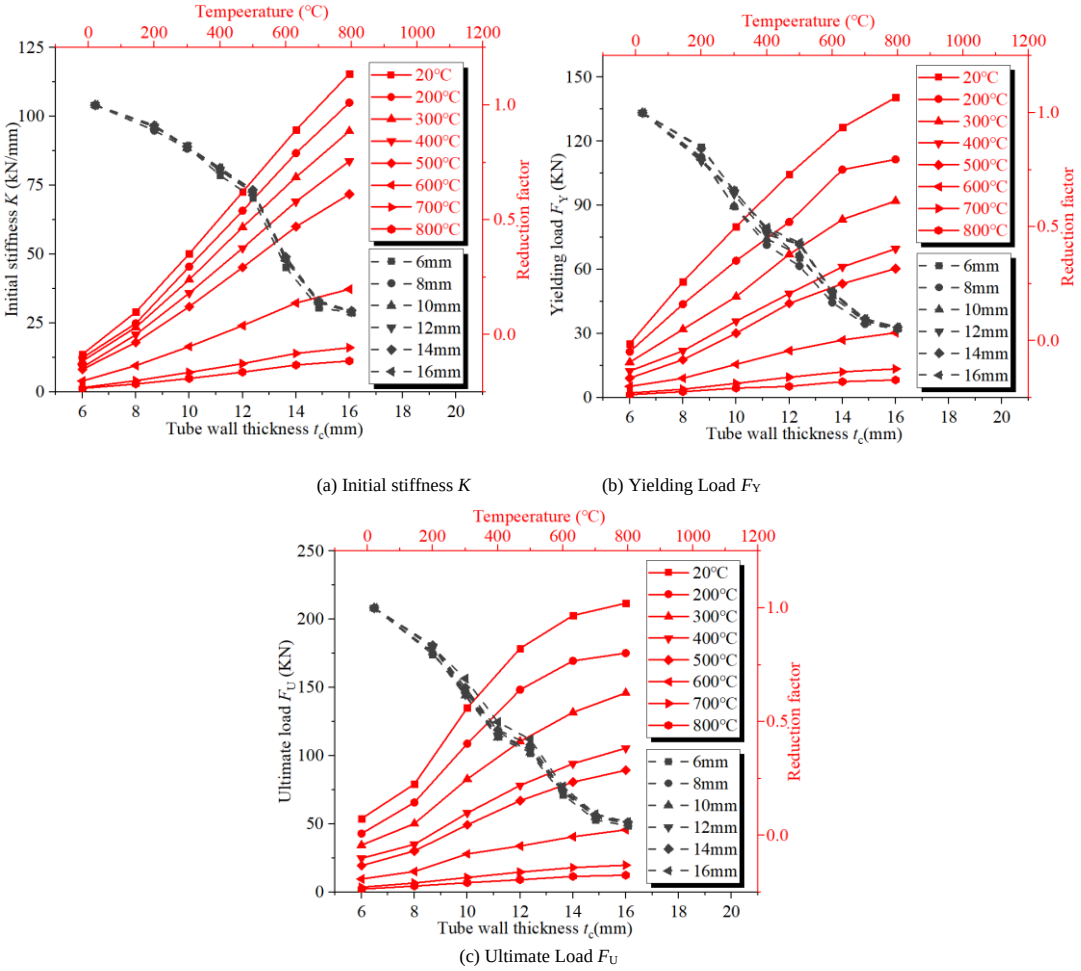

(a) Initial stiffness K (b) Yielding Load F_Y

(c) Ultimate Load F_U

Fig. 12 Influence of column thickness t_C on the tensile behavior of connections

3.2. Influence of preload

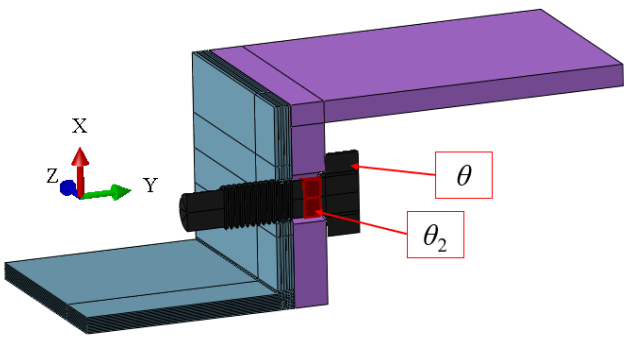

Fig. 13 Method to apply preload of bolt in FEM

Controlling the magnitude of the applied preload P is one of the key means to ensure the quality of bolted connections. An appropriately bolt preload P can make the bolt more effective in transferring loads and reliably connect the various components together. For TOB connections, in most cases, the strength of the threaded hole is inferior to that of a standard high-strength nut, and the tube wall thickness t_C is also typically less than the thickness of the nut. Therefore, it is necessary to research whether the bolt preload P can be applied to TOB in accordance with the requirements of Chinses code GB50017-2017 [26], and the influence of the preload P on the connection under different temperatures θ.

To consider the different degradation speeds of the elastic modulus E of ordinary structural steel and bolts under high fire temperatures on the bolt preload P, this paper applies the preload in the FEM by changing the temperature. Before applying the load to the model, imposing a different temperature θ_2 on a part of the bolt shaft than on other parts of the model. The temperature difference induces axial deformation in the bolt equivalent to the effect of the preload P. This simulates the impact of the bolt preload P on the load-bearing performance of the TOB connection, as shown in Fig. 13.

The distribution of stress and PEEQ inside the threaded hole after applying the bolt preload P, as obtained from the FEM, are shown in Fig. 14 and Fig. 15. After the application of preload P, the stress distribution within the threaded hole is nonuniform, decreasing from top to bottom. Under different temperatures θ, the plastic strain in the threaded hole caused by the pre-tension force does not exceed 0.02, indicating that the threads inside the hole remain in the elastic state.

Therefore, the specified preload P can be applied to TOB in accordance with the Chinese code GB50017-2017 [26] at different temperatures θ.

Two connection groups were analyzed as examples, with bolt diameter D being 16mm, T-stub flange thickness t_T being 12mm, and tube wall thicknesses

t_C being 6mm and 12mm respectively, the influence of bolt preload P on the TOB connection was analyzed. Fig. 16 compares the load-displacement curves of the two groups of connections before and after the application of bolt preload P. The changes in load-bearing performance, such as initial stiffness K, yield bearing capacity F_Y, and ultimate bearing capacity F_U, are listed in Table 3. The comparison reveals that after applying preload P, there is no significant change in the load-displacement curves, with only a slight increase in initial stiffness K that becomes less significant as temperature θ rises, nearly negligible above 400℃. The yield load F_Y and ultimate load F_U at different temperatures remain unchanged after the application of preload P. Furthermore, the bolt preload P does not change the failure mode of the connections.

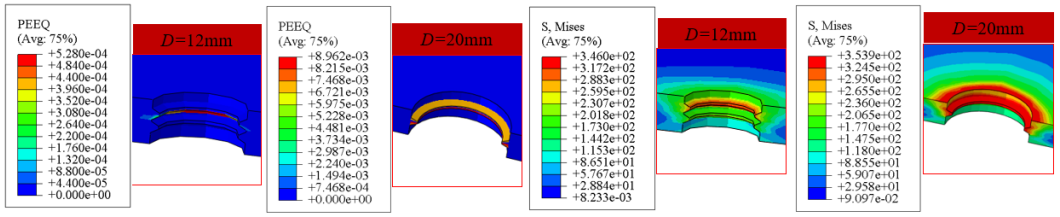

(a) θ=20℃

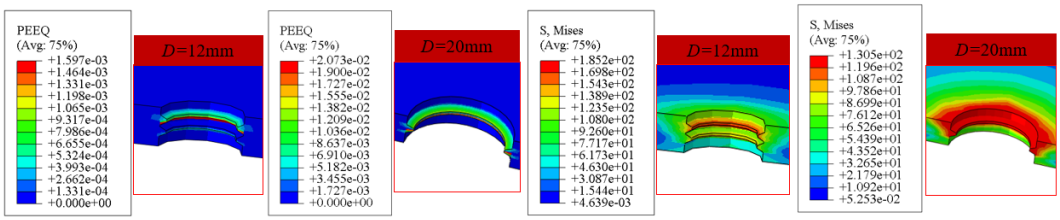

(b) θ=500℃

Fig. 14 Distribution of stress and strain inside bolt hole under preload P (t_C=6mm)

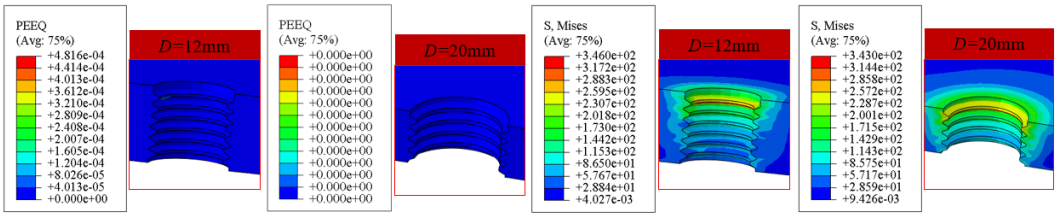

(a) θ=20℃

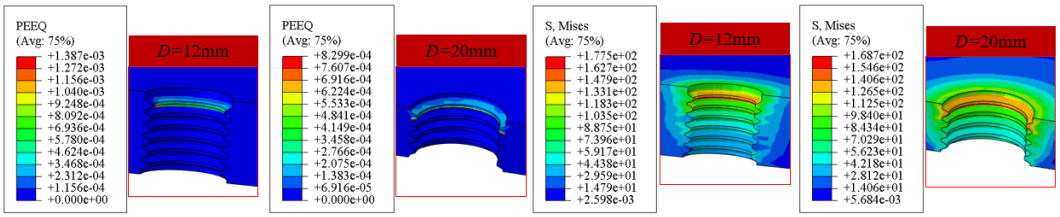

(b) θ=500℃

Fig. 15 Distribution of stress and strain inside bolt hole under preload P (t_C=12mm)

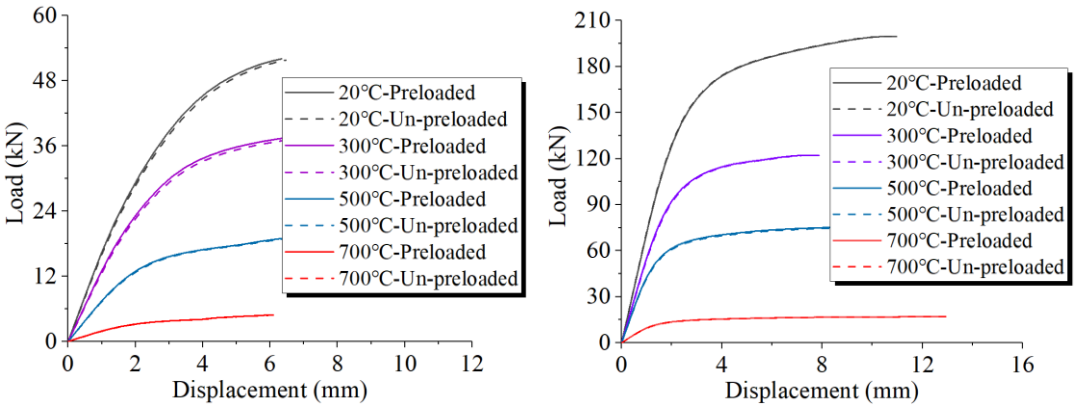

(a) t_C=6mm (b) t_C=12mm

Fig. 16 Comparison of preloaded and un-preloaded connections

Table 3
Comparison of preloaded and un-preloaded TOB connections

Temperature θ (℃)	Tube wall thickness t_c(mm)	Un-preloaded				Preloaded P			
		Initial stiffness K (kN/mm)	Yielding load F_Y(kN)	Ultimate Load F_U(kN)	Failure mode	Initial stiffness K (kN/mm)	Yielding load F_Y(kN)	Ultimate Load F_U(kN)	Failure mode
20	6	13.7	25.3	54.0	mode1	14.6	25.3	54.0	mode1
200		12.4	21.5	43.0	mode1	13.1	21.5	43.0	mode1
300		11.2	16.6	34.5	mode1	11.4	16.6	34.5	mode1
400		9.0	12.5	24.9	mode1	9.0	12.5	24.9	mode1
500		8.2	9.2	16.5	mode1	8.2	9.2	16.5	mode1
600		4.0	5.3	9.7	mode1	4.0	5.3	9.7	mode1
700		1.6	2.2	3.7	mode1	1.6	2.2	3.7	mode1
800		1.3	1.4	2.3	mode1	1.3	1.4	2.3	mode1
20	12	72.6	104.5	178.7	mode2	74.7	104.5	178.7	mode2
200		65.8	82.2	148.4	mode2	67.8	82.2	148.4	mode2
300		59.8	67.1	110.5	mode2	59.8	67.1	110.5	mode2
400		52.2	48.7	78.3	mode2	52.2	48.7	78.3	mode2
500		45.2	44.1	67.1	mode2	45.2	44.1	67.1	mode2
600		24.1	22.0	33.9	mode2	24.1	22.0	33.9	mode2
700		10.3	9.6	14.8	mode2	10.3	9.6	14.8	mode2
800		7.2	5.3	9.2	mode2	7.2	5.3	9.2	mode2

3.3. Influence of material properties

FEM simulations were conducted to analyze the influence of steel tube strength on the load-bearing performance under various temperatures θ. The analysis focused on connections composed of tube columns made from commonly used engineering materials: Q235, Q345, and Q460 steel grades. The analyzed connections all featured a bolt diameter (D) of 16mm, a tube section width (b_c) of 150mm, and a T-stub flange thickness (t_T) of 12mm. The materials of the T-stub and the steel tube were consistent, and the bolts were S8.8 high-strength bolts.

Fig. 17 compares the influence of tube material properties on the initial stiffness K. For connections with the same tube wall thickness (t_C), the initial stiffness K is essentially the same at a given temperature θ, and the reduction coefficient of initial stiffness K at different temperatures θ is also largely similar. This indicates that the initial stiffness K is primarily determined by dimensional parameters of the connection itself, such as the steel tube wall thickness (t_C). Changing the material of the steel tube does not influence the initial stiffness K of the connection.

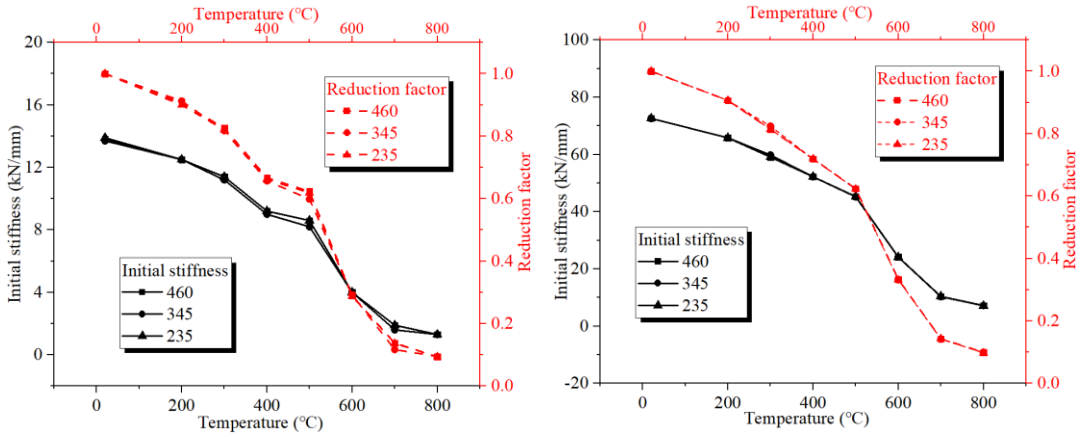

(a) t_C=6mm (d) t_C=12mm

Fig. 17 Influence of material property of steel tube on the initial stiffness K

Fig. 18 and Fig. 19 respectively compare the influence of material properties on the yield load (F_Y) and ultimate load (F_U). The comparison shows that the material properties have a significant influence on the load-bearing capacity of the connection. Taking the connection with a tube wall thickness (t_C) of 6mm as an example: when the steel tube material is Q235, Q345, and Q460, the yield load F_Y at ambient temperature is 13.2kN, 18.1kN, and 23.5kN, respectively, and the ultimate load F_U is 27.7kN, 38.5kN, and 49.9kN, respectively. Compared to the Q235 steel material connections, the Q345 steel material connections show an increase of 37% and 39% in F_Y and F_U, respectively, while the Q460 steel material connections exhibit increases of 78% and 80% in F_Y and F_U, respectively. For other connections with different tube wall thicknesses t_C, the pattern of material performance affecting their load-bearing capacity is essentially consistent, as shown in Fig. 18 and Fig. 19.

As the temperature θ increases, there is a rapid decrease in the load-bearing capacity of the connections. When the fire temperature θ rises to 500°C, both the yielding load (F_Y) and the ultimate load (F_U) of the connections decreased to approximately 50% of their capacity at ambient temperatures. Furthermore, as the temperature θ further increases to 700°C, the load-bearing capacity of the connections declines to about 10% of the ambient temperature capacity, indicating a near-total loss of load-bearing ability. In this case, although enhancing the strength grade of the steel can marginally increase the load-bearing capacity of the connections, this improvement is negligible.

Fig. 18 and Fig. 19 also compare the reduction factors of the load-bearing capacity of connections at varying temperatures θ. It is observed that changing the material strength does not affect the deterioration speed of the yielding load (F_Y) and ultimate load (F_U). Moreover, while changing the material strength of the connections significantly improves their load-bearing capacity, it does not result in a change in the failure mode of the connections.

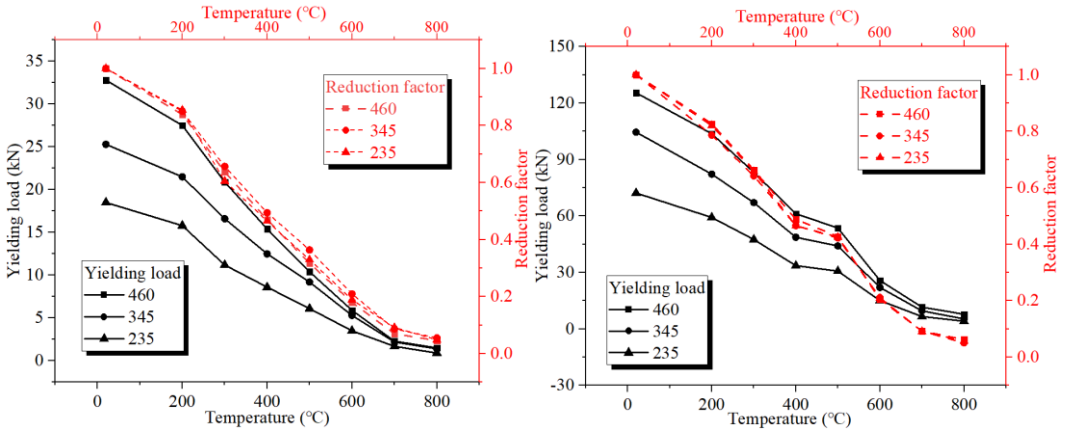

(a) t_C=6mm (d) t_C=12mm

Fig. 18 Influence of material property of steel tube on yielding load F_Y

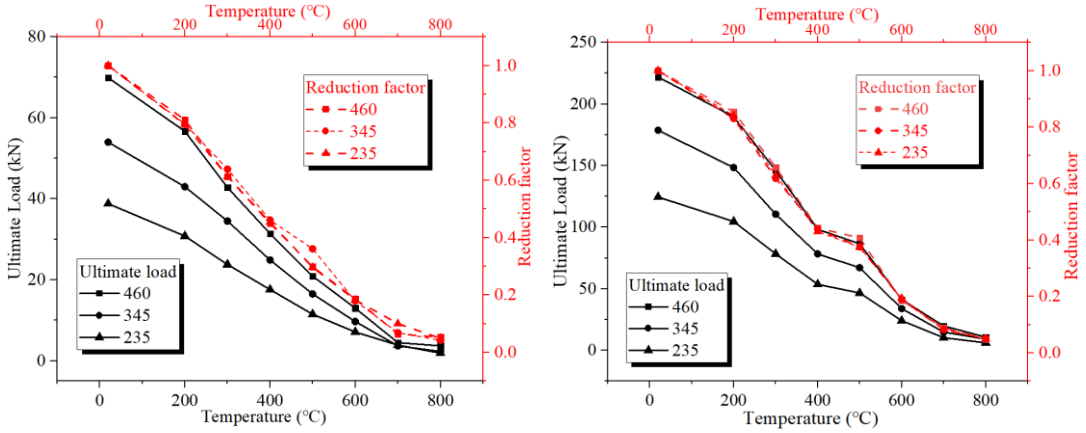

(a) t_C=6mm (d) t_C=12mm

Fig. 19 Influence of material property of steel tube on ultimate load F_U

Table 4
Comparison of connections with different tube materials

Tube wall thickness t_c(mm)	Temperature θ(°C)	Initial stiffness K (kN/mm)			Yielding load F_Y(kN)			Ultimate Load F_U(kN)			Failure mode		
		235	345	460	235	345	460	235	345	460	235	345	460
6	20	13.9	13.7	13.8	18.5	25.3	32.8	38.8	54.0	69.9	mode1	mode1	mode1
	200	12.5	12.5	12.5	15.8	21.5	27.5	30.8	43.0	56.7	mode1	mode1	mode1
	300	11.4	11.2	11.4	11.2	16.6	20.9	23.8	34.5	42.8	mode1	mode1	mode1
	400	9.2	9.0	9.2	8.6	12.5	15.4	17.6	24.9	31.4	mode1	mode1	mode1
	500	8.6	8.2	8.6	6.1	9.2	10.4	11.5	16.5	20.9	mode1	mode1	mode1
	600	4.0	4.0	4.0	3.5	5.3	5.9	7.1	9.7	13.0	mode1	mode1	mode1
	700	1.9	1.6	1.9	1.7	2.2	2.3	3.9	3.7	4.5	mode1	mode1	mode1
	800	1.3	1.3	1.3	0.9	1.4	1.5	1.9	2.3	3.7	mode1	mode1	mode1
12	20	72.6	72.6	72.6	72.2	104.5	125.4	124.5	178.7	221.9	mode2	mode2	mode2
	200	65.8	65.8	65.8	59.2	82.2	103.7	104.6	148.4	189.6	mode2	mode2	mode2
	300	59.1	59.8	59.1	47.5	67.1	83.2	78.3	110.5	146.0	mode2	mode2	mode2
	400	52.2	52.2	52.2	33.6	48.7	61.2	53.6	78.3	98.3	mode2	mode2	mode2
	500	45.2	45.2	45.3	30.7	44.1	53.6	46.6	67.1	86.5	mode2	mode2	mode2
	600	24.1	24.1	24.2	15.1	22.0	25.7	24.1	33.9	41.3	mode2	mode2	mode2
	700	10.4	10.3	10.4	6.6	9.6	11.6	10.3	14.8	19.8	mode2	mode2	mode2
	800	7.1	7.2	7.2	4.1	5.3	7.8	6.2	9.2	10.8	mode2	mode2	mode2

3.4. Influence of internal constraint component

Closed-section steel columns exhibit superior torsional and flexural properties, hence the wall thickness (t_C) is typically quite small. To prevent premature failure of the connections compared to other components, it may be necessary to reinforce the connection regions of steel tube columns. Additionally, the tube wall thickness (t_C) is a critical parameter that directly influences the failure mode and load-bearing capacity of TOB connections. Therefore, to ensure the effectiveness of TOB connections, reinforcing the connection areas is also essential. One approach to strengthening these areas involves installing an Internal Constraint Component (ICC) inside the steel tube, such as an H-shaped steel.

The installation of the ICC can be carried out as follows, as illustrated in Fig. 20:

1. Cut openings in the column at the connection area to serve as plug welding holes.
2. Insert the ICC into the specified position.
3. Temporarily weld the ICC in place through the plug welding holes.
4. Create threaded holes penetrating both the steel tube column and the ICC.

This method addresses the challenges of limited construction space in closed-section steel tube columns. It ensures reliable fixation of the ICC within the steel tube and guarantees the quality of threaded hole machining, preventing issues like misalignment of bolt holes or discontinuous threads.

However, it is inevitable that there will be a gap between the ICC and the column wall, resulting in discontinuity of the hole threads. Moreover, the stress distribution on the bolt shank is not uniform, leading to discontinuous deformation and load distribution between the ICC and the column wall. Consequently, it is essential to research how the ICC and the column wall work together and to evaluate the reinforcing effect of the ICC on the TOB connections.

FEM analysis has been conducted to assess the load-bearing performance of TOB connections utilizing H-shaped steel as the ICC. The studied connections had a tube wall thickness (t_C) of 6mm, a bolt diameter (D) of 16mm, a T-stub flange thickness (t_T) of 12mm, and an H-shaped steel flange thickness (t_H) ranging from 6mm to 16mm.

With the increase in the flange thickness of the H-shaped steel (t_H), the reinforcing effect of the ICC on the connection gradually increases. Consequently, the failure mode of the connection changes from tube column wall yielding (mode 1) to T-stub flange yielding accompanied by bolt failure (mode 2). For H-shaped steel flange thicknesses (t_H) below 12mm (equivalent to twice the tube wall thickness t_C), the connections typically exhibit failure mode 1. Conversely, when the flange thickness (t_H) of the H-shaped steel is 12mm or more, the connections exhibit failure mode 2. Fig. 21 and Fig. 22 show the stress distribution and the PEEQ within the threaded holes of the connection when the yielding load F_Y is reached. It is observed that the stress distribution inside the threaded holes of the connection is nonuniform, with overall stress in the threaded holes on the H-shaped steel flange being greater than that on the steel tubular column. This indicates that the H-shaped steel provides additional anchorage force for the TOB. Moreover, under the yielding load F_Y, only minor PEEQ occurs locally in the threaded holes of both the H-shaped steel and the steel tubular column, suggesting that the threaded holes still effectively provide reliable anchoring for the bolts.

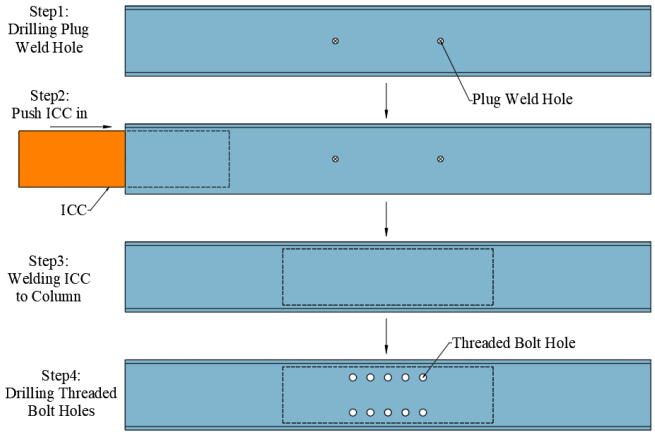

Fig. 20 Progress of installing the ICC inside the column

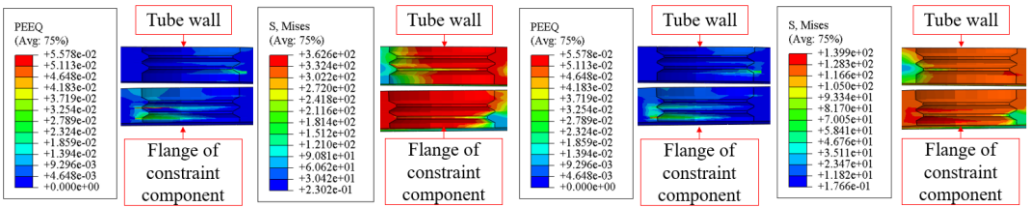

(a) θ=20℃ (b) θ=500℃

Fig. 21 State of the hole threads under yielding load F_Y (t_H=6mm)

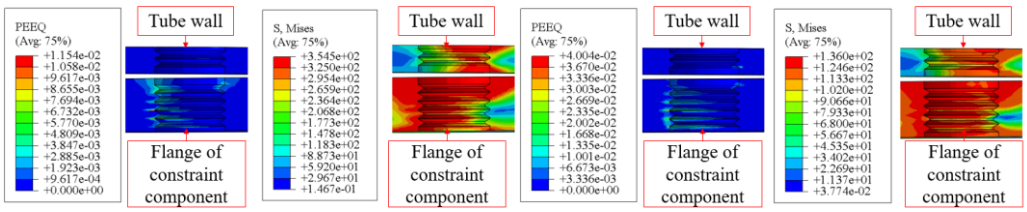

(a) θ=20℃ (b) θ=500℃

Fig. 22 State of the hole threads under yielding load F_Y (t_H=12mm)

Fig. 23 compares the relationship between the initial stiffness K, yielding load F_Y, and ultimate load F_U of the connection with the flange thickness t_H of the H-shaped steel. When t_H does not exceed 12mm, initial stiffness K, yielding load F_Y, and ultimate load F_U of the connection all increase rapidly with the increase of t_H. However, once t_H reaches 12mm, the influence becomes minimal. This is attributed to a change in the failure mode of the connection. Below 12mm t_H, the failure mode is tube column wall yielding (mode 1), where the load-bearing performance of the connection is determined by the resistance tube column wall. For larger t_H values, the failure mode changes to T-stub flange yielding accompanied by bolt failure (mode2). In this case, the resistance of the column wall to out-of-plane deformation exceeds the bending resistance of the T-stub flange. As a result, further increases in t_H less influential on the load-bearing capacity of the connection. Despite the significant differences in stiffness and load-bearing performance among connections with varying t_H, their degradation under high temperatures are similar. Fig. 23 shows that the degradation speed of initial stiffness K, yielding load F_Y, and ultimate load F_U at high temperatures are consistent across different connections.

Taking connections with t_H of 6mm and 12mm as examples, the impact of the material strength of the ICC on the connection was compared, as shown in Fig. 25. The strength of the ICC has no significant effect on the initial stiffness K of the connection. However, the material strength of the ICC significantly influences the yielding load F_Y and ultimate load F_U of the connection at different temperatures. For instance, at a temperature θ of 20°C, increasing the strength of the ICC from Q235 to Q460 led to an increase of 84% and 86% in the yielding load F_Y and ultimate load F_U, respectively for a connection with t_H of 6mm. For a connection with a t_H of 12mm, the increases were 41% in F_Y and

38% in F_U. Nonetheless, changing the strength of the ICC did not alter the failure mode of the connection, nor did it significantly change the degradation speed of the yielding load F_Y and ultimate load F_U at high temperatures.

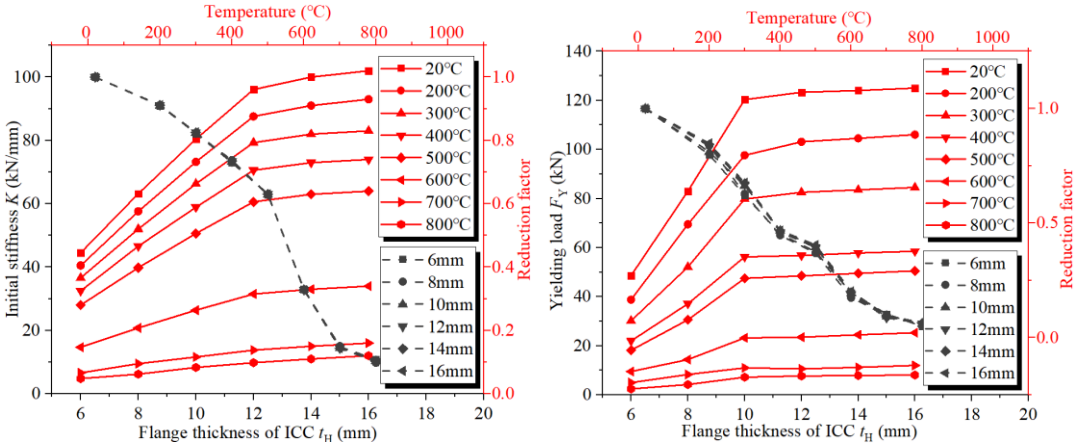

(a) Initial stiffness K (b) Yielding Load F_Y

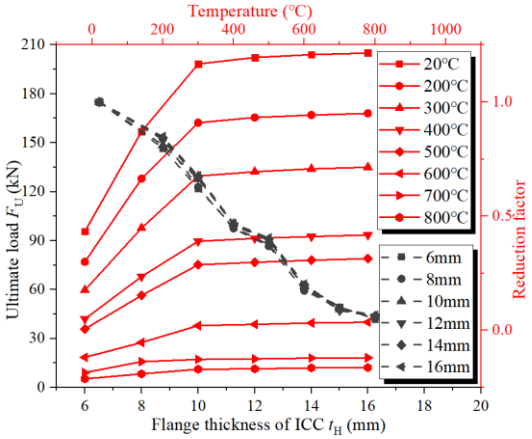

(c) Ultimate Load F_U

Fig. 23 Influence of flange thickness of ICC t_H on the tensile behavior of connections

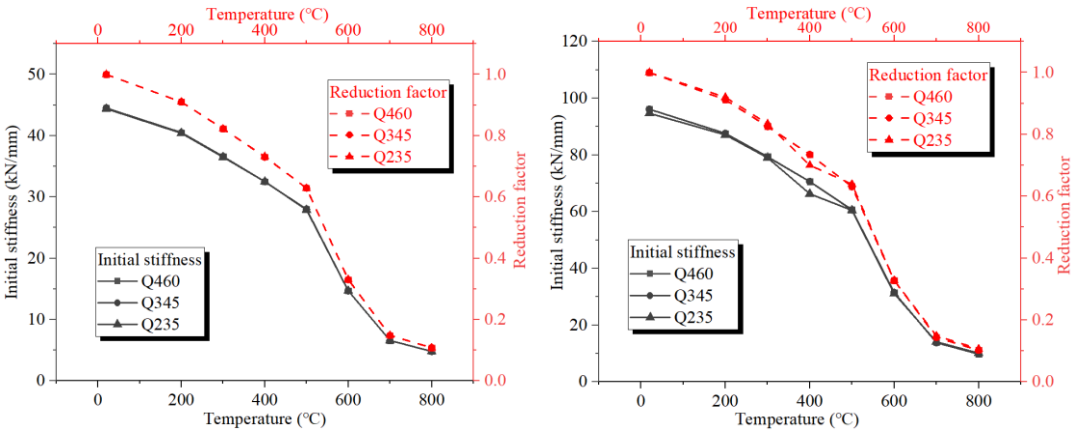

(a) t_C=6mm (d) t_C=12mm

Fig. 24 Influence of material property of ICC on initial stiffness K

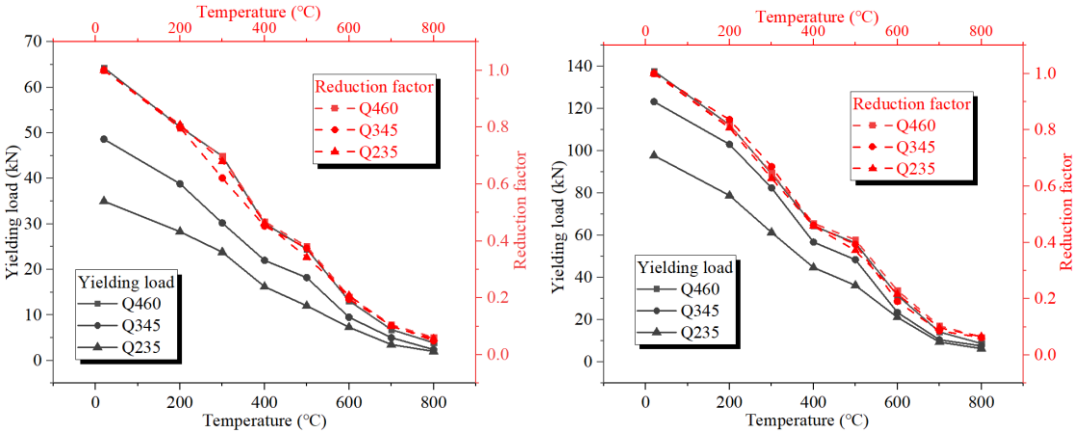

(a) t_C=6mm (d) t_C=12mm

Fig. 25 Influence of material property of ICC on yielding load F_Y

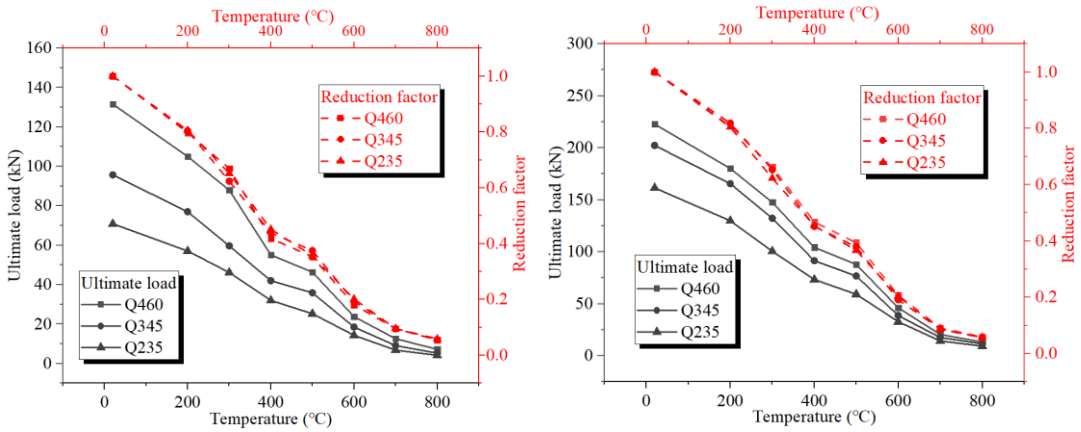

(a) t_C=6mm (d) t_C=12mm

Fig. 26 Influence of material property of ICC on ultimate load F_U

4. Calculation of the tensile resistance

4.1. Calculation method for failure mode 1

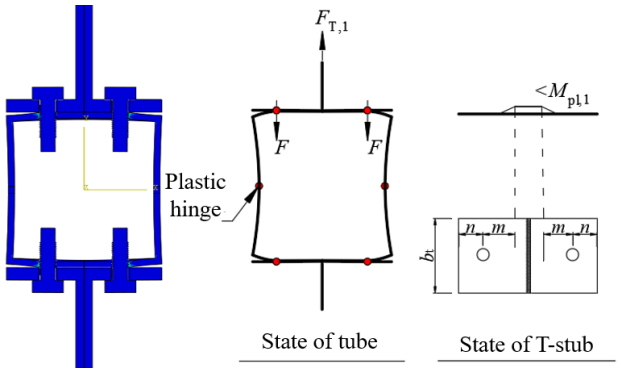

Fig. 27 Calculation model of mode 1

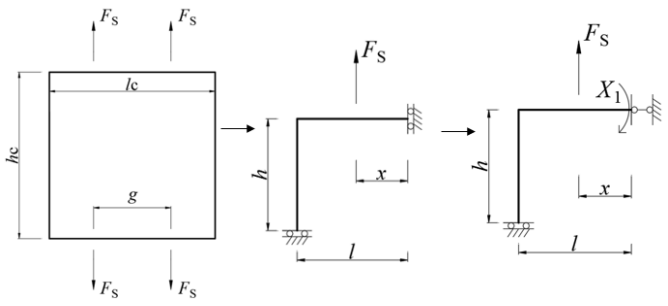

Fig. 28 Simplified calculation model

When the connection exhibits failure mode 1, characterized by tube column wall yielding, the primary features include minor deformation of the T-stub and significant out-of-plane deformation of the steel tube wall. The deformation of the steel tube sidewalls is predominantly horizontal, while the top and bottom surfaces mainly exhibit vertical deformation. Based on the deformation characteristics of the steel tube, a simplified computational model can be established as shown in Fig. 27. Due to the symmetry of the connection, a quarter-section of the steel tube structure with sliding supports at both ends can be use for analyzing, as shown in Fig. 28.

The simplified quarter model is subjected to a concentrated force, F_S, at the bolt axis position, with a height of h and a length of l, and the distance from the concentrated force F_S to the sliding support is x. Since this simplified model constitutes a statically indeterminate structure, it cannot be directly solved using conditions of static equilibrium and moment balance. Instead, the method of forces from structural mechanics can be applied, decomposing a sliding support into a hinged support and an equivalent bending moment X, as shown in Fig. 28. The deformations under the concentrated force F_S and under the bending moment X can then be determined using the principle of virtual work.

By ensuring deformation compatibility at the sliding supports before and after simplification, a new equilibrium equation (4) can be established. Solving this equation yields the magnitude of the bending moment X_1, which in turn allows for the construction bending moment diagram of the entire steel frame.

$$\delta X + \Delta_F = \Delta \tag{4}$$

Here δ is the angle of rotation at the sliding support when X=1, representing the structural flexibility coefficient under the action of bending moment X; Δ_F is the angle of rotation of the structure in the direction of bending moment X caused by the external force F_S; Δ is the actual displacement at the point of release of the redundant support in the original structure. Since the sliding support in the original structure do not allow rotation, Δ is zero at this point.

The bending moment diagrams under the bending moment X=1 and under the action of the concentrated force F_S are shown in Fig. 29. Then, according to the principle of virtual work, it can be determined:

$$\delta = \int_0^l \frac{1\times 1}{EI} ds + \int_0^l \frac{1\times 1}{EI} ds = \frac{2l}{EI} \tag{5}$$

$$\Delta_F = \int_0^l \frac{F_S \times (l-x)}{EI} ds + \int_{l-x}^l \frac{F_S \times s}{EI} ds = \frac{1}{EI} Fl(l-x) + \frac{1}{2EI} x(2l-x) \tag{6}$$

By combining Eqs (4), (5), and (6), it can be derived that:

$$X = \frac{F_S(l-x)}{2} + \frac{F_S x(2l-x)}{4l} \tag{7}$$

By superimposing the bending moment diagrams in Fig. 29, the bending moment diagram for the original steel frame can be obtained, as shown in Fig. 30. Furthermore, this allows for the determination of the magnitude of the bending moment M_H at the sliding support in the upper right corner of the steel frame:

$$M_H = \frac{F_S(l-x)}{2} + \frac{F_S x(2l-x)}{4l} \tag{8}$$

FEM results indicate that significant deformation occurred both at the bolt axis and at the midpoint of the side wall of the steel tube, suggesting that yielding has likely occurred at these locations. Therefore, by isolating the section at the sliding support, the stress distribution can be observed as shown in Fig. 31. In the area affected by M_H, there is no axial force influence, and the equilibrium conditions of the isolated section yield the following:

$$M_H = \frac{f_y l_{eff} t_c^2}{4} \tag{9}$$

Here, l_{eff} is the length of yield line. By combining Equations (8) and (9), it can be obtained that:

$$F_S = \frac{f_y l_{eff} t_C^2 l}{2l^2 - x^2} \tag{10}$$

The above derivation is based on the premise of minimal deformation of the connection. However, in reality, connections that exhibit failure mode 1 have relatively thin steel tube walls and exhibit significant out-of-plane deformation upon yielding. This deformation is especially pronounced at high temperatures, where the elastic modulus of the connection rapidly decreases, leading to even more pronounced deformation. Therefore, the impact of large deformations on the load-bearing capacity of the connection cannot be ignored. When failure mode 1 occurs, the deformation of the connection primarily consists of inward horizontal displacement of the side walls and outward vertical displacement of the top and bottom surfaces, denoted as Δ_V and Δ_H, respectively, as shown in Fig. 32. In the case of small deformations, the following equilibrium equation can be obtained:

$$M_H = M_V + F(l-x) \tag{11}$$

In the case of large deformations, the following equilibrium equation can be established:

$$M_{H,large} = M_{V,large} + F_{large}(l - x - \Delta_V) \tag{12}$$

Assuming that large deformations of the connection only alter the magnitude of the bending moment without changing the distribution pattern of the bending moment diagram, that is:

$$\frac{M_{H,large}}{M_{V,large}} = \frac{M_H}{M_V} \tag{13}$$

By combining Eqs (11), (12), and (13), it can be derived that:

$$F_{S,large} = \frac{1 - x - \Delta_V}{1 - x} F_S \tag{14}$$

Therefore, the bearing capacity reduction coefficient k_Δ considering the influence of large deformation can be obtained:

$$k_\Delta = \frac{1 - x - \Delta_V}{1 - x} \tag{15}$$

To determine the value of k_Δ, it is also necessary to determine the magnitude of Δ_V. In order to simplify the calculation, it is assumed that Δ_V is 3% of the width of the tube, that is:

$$\Delta_V = 0.03 b_C \tag{16}$$

Here, b_c is the width of the tube. Considering the strength reduction of steel at high temperatures, the calculation method of bearing capacity of the connection at high temperature $F_{S,\theta}$ considering large deformation can be obtained:

$$F_{S,\theta} = \Delta_V \frac{f_{y,\theta} l_{eff}^2 t_C^2 l}{2l^2 - x^2} \tag{17}$$

$$F_{T,1} = 2F_S \tag{18}$$

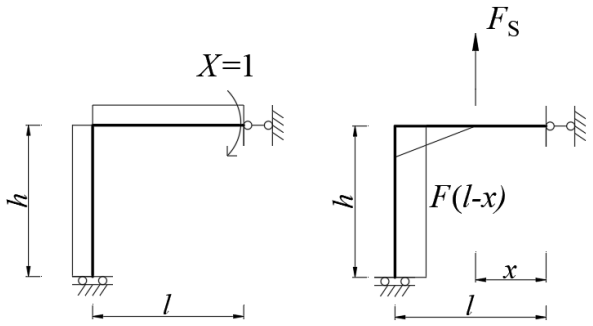

Fig. 29 The bending moment diagram under X=1 and F_S

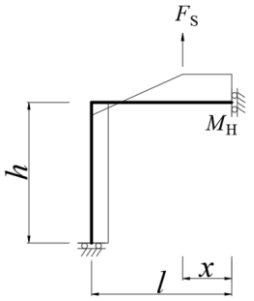

Fig. 30 The solved bending moment diagram of the steel frame

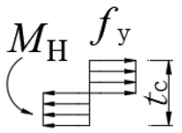

Fig. 31 The stress distribution of the section near the support

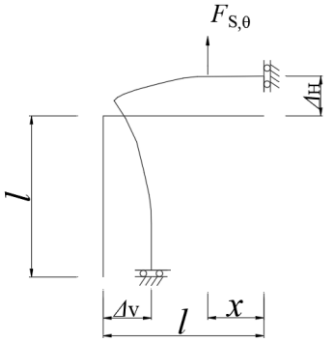

Fig. 32 The frame under large deformation

4.2. Calculation method for other failure modes

When the connection exhibits failure mode 2, T-stub flange yielding accompanied by bolt failure, the deformation of the steel tube is minor. The deformation is primarily concentrated on the T-stub, where a yield line forms at the junction between the web and flange of the T-stub. Simultaneously, the bolt reaches its maximum load-bearing capacity and fractures. The internal energy consumed by the yield line is:

$$M_{pl}=0.25l_{eff}t_t^2 f_y \tag{19}$$

By separately analyzing the flange of the T-stub, it can be considered as a beam, with its bending moment diagram shown in Fig. 33. Additionally, the beam is subjected to the combined effects of the external force $F_{T,2}$, the prying force Q, and the bolt tension F_b. From the conditions of static equilibrium, it can be derived that:

$$F_{T,2}+2Q=2F_b \tag{20}$$

Additionally, the balance condition of the bending moment at the junction between the T-stub flange and the web can be obtained as follows:

$$M_{pl}=mF_b-(m+n)Q \tag{21}$$

where m and n are the dimensional parameters of the T-stub, as shown in Fig. 33.

By combining Eqs (19), (20), and (21), and eliminating the prying force Q, the load-bearing capacity $F_{T,2}$ of failure mode 2 can be obtained:

$$F_{T,2}=\frac{2nF_b+2M_{pl}}{m+n} \tag{22}$$

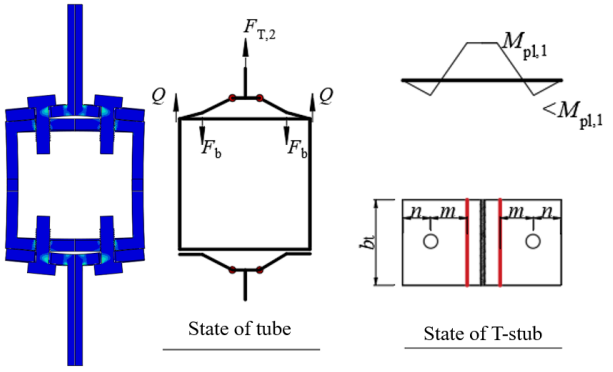

Fig. 33 Calculation model of the connection failed by mode 2

Through a similar method, the load-bearing capacity of connections exhibiting failure mode 3 can also be derived. When the connection experiences failure mode 3, characterized by T-stub flange yielding, the deformation of the steel tube is minimal, while the deformation of the T-stub flange is more pronounced. Yield lines occur at the intersection of the web and flange of the T-stub as well as at the bolt holes, leading to the simplified calculation model shown in Fig. 34. The T-stub is simplified as a beam for analysis, subjected to the combined effects of a prying force Q, external force $F_{T,3}$, and bolt tension F_b, where the bending moment diagram is characterized by reaching M_{pl} at both the positions corresponding to the bolt holes and at the intersection of the T-stub web and flange. Thus, through the conditions of static equilibrium and bending moment equilibrium, it can be obtained that:

$$F_{T,3}+2Q=2F_b \tag{23}$$

$$M_{pl}=mF_b-(m+n)Q \tag{24}$$

$$M_{pl}=Qn \tag{25}$$

By combining Eqs (23), (24), and (25), it can be derived that:

$$F_{T,3}=\frac{4M_{pl}}{m} \tag{26}$$

When the connection exhibits failure mode 4, bolt fracture failure, the deformation of both the steel tube and the T-stub is relatively minor, and the load-bearing capacity of the connection is solely determined by the load-bearing capacity of the bolt. The model for calculating this type of connection is shown in Fig. 35. The equation for calculating its load-bearing capacity is:

$$F_{T,4}=\sum F_b \tag{27}$$

$$F_b=\frac{\pi d^2}{4} f_{yb} \tag{28}$$

where d is the effective diameter of the bolt, and $f_{y,b}$ is the yield strength of the bolt.

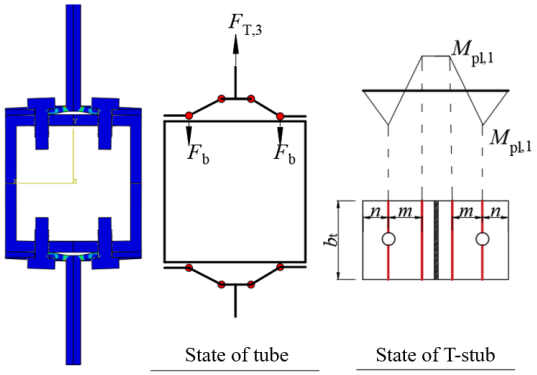

Fig. 34 Calculation model of the connection failed by mode 3

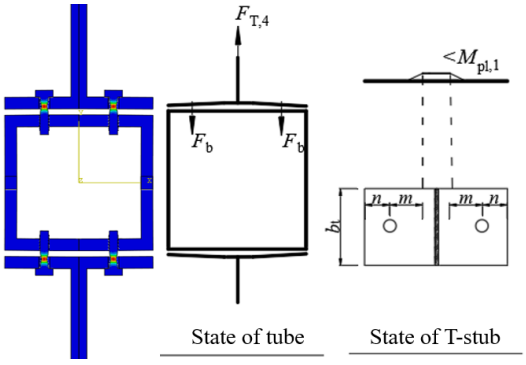

Fig. 35 Calculation model of the connection failed by mode 4

4.3. Calculation method for connections with ICC

For connections with ICC, the potential failure modes are the same as those without ICC. When the connection experiences failure modes 2, 3, or 4, the location of failure is independent of the ICC, thus the calculation method remains the same as for the connections without ICC. However, when failure mode 1 occurs, the cooperative action between the ICC and the steel tube must be considered. FEM analysis reveals that for connections with ICC experiencing failure mode 1, the out-of-plane deformation of the tube wall is significantly restricted upon reaching its yield load F_Y, and both the bolts and T-stub remain in the elastic state. Based on these characteristics, the following assumptions can be mad:

1. Ignore the effect of the plug welding between the ICC and the tube wall;
2. Ignore the axial deformation of the bolt in the ICC and the tube wall;
3. Ignore the out-of-plane deformation of the steel tube sidewall.

In calculations, both the steel tube wall and the ICC are treated as beam to establish the calculation model shown in Fig. 36.

The deformations produced at the bolt axis by the tube wall and the ICC are denoted as δ_{SHS} and δ_H, respectively. Given that the axial deformation of the bolt shank in the gap between the tube and the ICC is neglected, the following deformation compatibility relationship is established:

$$\delta_{SHS} = \delta_H \tag{29}$$

In addition, based on the equilibrium of forces:

$$F_S = F_{SHS} + F_H \tag{30}$$

Where F_S is the total anchorage of the threads within the hole, which is also equal to the axial force on the bolt shank; F_{SHS} is the load carried by the threaded holes of the tube; F_H is the load carried by the threaded holes of the H-shaped steel flange, acting as the ICC. Based on the unit load method, which relies on the principle of virtual work, expressions for δ_{SHS} and δ_H can be separately derived. The derived expression for δ_H is as follows:

$$\delta_H = \frac{F_H l x^2}{6EI_H}(3 - \frac{x}{l}) \tag{31}$$

$$I_H = \frac{b_H t_H^2}{12} \tag{32}$$

I_H, b_H, and t_H represent the moment of inertia for bending resistance, width, and flange thickness of the ICC, respectively. The expression for δ_{SHS} is as follows:

$$\delta_{SHS} = \frac{1}{EI_{SHS}}(\frac{2}{3}F_{SHS}(l-x)^3 + \frac{F_{SHS}(l-x)^4(2x-l)}{4l^2}) \tag{33}$$

$$I_{SHS} = \frac{b_c t_c^2}{12} \tag{34}$$

I_{SHS}, b_c, and t_c represent the moment of inertia for bending resistance, width, and thickness of the tube wall, respectively. Through Equations (29) and (30), the relationship between F_{SHS} and F_H can be established:

$$F_{SHS} = 2\frac{I_{SHS}}{I_H}\frac{l^2x^2(3l-x)}{8(l-x)^3l^2 + 3(l-x)^4(2x-l)}F_H \tag{35}$$

Hence, the influence coefficient k_H of ICC is:

$$k_H = \frac{F_S}{F_{SHS}} = \frac{F_{SHS} + F_H}{F_{SHS}} = \frac{(8(l-x)^3l^2 + 3(l-x)^4(2x-l))I_H + 2l^2x^2(3l-x)I_{SHS}}{2l^2x^2(3l-x)I_{SHS}} \tag{36}$$

Given that the effect of plug welding is not considered, the ICC and the tube only transfer load through bolts, thus the ICC does not change the bending moment distribution pattern of the tube wall but only changes its magnitude. Therefore, Eq (17) can still be applied to solve for the bending moment on the tube column, leading to the conclusion that:

$$F_S = k_H \frac{f_y l_{eff} t_c^2 l}{2l^2 - x^2} \tag{37}$$

$$F_{T,1} = 2F_S \tag{38}$$

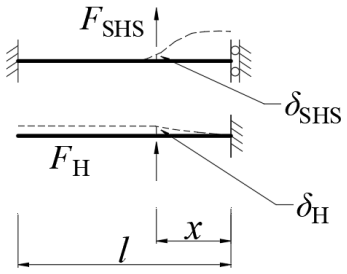

Fig. 36 Calculation model for the connection with ICC failed by mode 1

4.4. Accuracy analysis of calculation methods

The calculated load F_E of the connections at different temperatures θ using the derived equations, compared with the yielding load F_Y obtained from FEM calculations are shown in Fig. 37. It is observed that for TOB connection without ICC, the calculated load F_E at different temperatures θ derived from the equations closely matches the yielding load F_Y obtained from the FEM, with an average F_E to F_Y ratio of 1.012, a standard deviation of 0.084, and a coefficient of variation of 0.083. For connections with ICC, the disparity between calculated load F_E and the yielding load F_Y obtained from FEM is slightly larger, with an average F_E to F_Y ratio of 0.969, a standard deviation of 0.121, and a coefficient of variation of 0.125. However, the overall accuracy remains satisfactory.

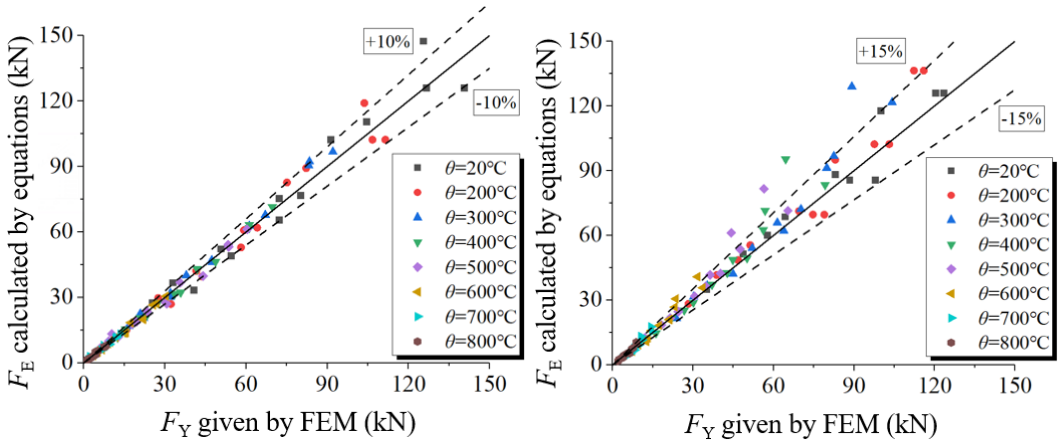

(a) connections without ICC (b) connections with ICC

Fig. 37 Comparison of the simulation result and calculation results

5. Conclusions

This study developed and validated a finite element model to analyze the mechanical performance of T-stub to steel tube connections bolted by TOB under high-temperature conditions. The key findings and contributions are as follows:

(1) Based on the parameters of the connection, there are four potential failure modes for TOB connections: tube column wall yielding (mode1), T-stub flange yielding accompanied by bolt failure (mode2), T-stub flange yielding (mode3), and bolt fracture failure (mode4).

(2) Bolt preload forces, as per the Chinese Code GB50017-2017, slightly enhance the initial stiffness of the connection but have minimal influence on the load-bearing capacity. The influence of preload diminishes as temperature increases.

(3) The failure mode and initial stiffness of the connection are influenced by dimensional parameters but are less affected by the tube strength. Steel

strength improvement significantly enhances the yielding and ultimate load, though its influence diminishes at higher temperatures.

(4) Installing Internal Constraint Components (ICC) effectively enhances connection performance, especially for tubes with smaller wall thicknesses. The material strength and flange thickness of ICCs significantly influence the stiffness and failure mode of the connection.

(5) A method for calculating the load-bearing capacity of TOB connections under high temperatures has been introduced and validated through comparisons with FEM results. The proposed method accurately predicts the yielding load capacity of TOB connections, both with and without ICC, across different temperature conditions.

Acknowledgments

This paper was supported by the Natural Science Foundation of Shandong Province (ZR2023QE324, ZR2024ME215).

Nomenclatures and variables

F_y	Yielding load
F_u	Ultimate load
F_T	calculated tension resistance
M_{pl}	bending strength of T-stub flange
$l_{eff,f}$	length of the yielding line
t_f	thickness of T-stub flange
b	width of the T-stub
m	distance between weld toe and bolt hole
e	end distance of T-stub flange
TOB	Thread-fixed One-side Bolt
TB	Traditional Bolt
FEM	Finite Element Model
PEEQ	plastic equivalent strain

References

[1] You Y, Li Y, Lin C, et al. Post-fire behavior of square hollow section column connections using thread-anchored blind bolts[C]//Structures. Elsevier, 2024, 59: 105706.

[2] Lindapter. Type HB – Hollo-bolt. Cavity fixings 2, Product brochure. UK: Lindapter International; 2012. p. 41–3.

[3] Wang Z Y, Wang Q Y. Yield and ultimate strengths determination of a blind bolted endplate connection to square hollow section column[J]. Engineering structures, 2016, 111: 345-369.

[4]. Cabrera M, Tizani W, Ninic J, et al. Experimental and numerical analysis of preload in Extended Hollo-Bolt blind bolts[J]. Journal of Constructional Steel Research, 2021, 186: 106885.

[5] Pan H, Chen J, Liu Y. Low-cycle fatigue behavior on the tensile region of Hollo-bolted angle connections[J]. Journal of Constructional Steel Research, 2023, 208: 107967.

[6] Pascual A M, Romero M L, Tizani W. Fire performance of blind-bolted connections to concrete filled tubular columns in tension[J]. Engineering Structures, 2015, 96: 111-125.

[7] Pascual A M, Romero M L, Tizani W. Thermal behaviour of blind-bolted connections to hollow and concrete-filled steel tubular columns[J]. Journal of Constructional Steel Research, 2015, 107: 137-149.

[8] Song T Y, Tao Z, Razzazzadeh A, et al. Fire performance of blind bolted composite beam to column joints[J]. Journal of Constructional Steel Research, 2017, 132: 29-42.

[9] Lee J, Goldsworthy H M, Gad E F. Blind bolted T-stub connections to unfilled hollow section columns in low rise structures[J]. Journal of Constructional Steel Research, 2010, 66(8-9): 981-992.

[10] Hosseini S M, Mamun M S, Mirza O, et al. Behaviour of blind bolt shear connectors subjected to static and fatigue loading[J]. Engineering Structures, 2020, 214: 110584.

[11] BS EN 1993-1-8. Design of Steel Structures - Part 1-8: General Rules - Design of Joints. European Committee for Standardization, Brussels (2005)

[12] Wan C, Bai Y, Ding C, et al. Mechanical performance of elliptical one-sided joints: Loading direction and bolt row effects[J]. Journal of Constructional Steel Research, 2022, 197: 107461.

[13] Sun L, Liu M, Liu Y, et al. Studies on T-shaped one-side bolted connection to hollow section column under bending[J]. Journal of Constructional Steel Research, 2020, 175: 106359.

[14] Li Y L, Zhao X L. Study on stainless steel blind bolted T-stub to concrete-filled stainless steel tube connections[J]. Engineering Structures, 2022, 257: 114107.

[15] Fan S, Wang J, Duan S, et al. Experimental study on forming mechanism and mechanical properties of novel self-tightening one-side bolt[J]. Engineering Structures, 2023, 283: 115915.

[16] You Y, Li Y, Lin C, et al. Postfire Performance of Thread-Anchored Blind-Bolted Connection[J]. Journal of Structural Engineering, 2023, 149(12): 04023173.

[17] You Y, Zhang S, Xing D, et al. Study on tensile behavior and design methods of thread-fixed one-side bolted joints to concrete-filled steel tubes[J]. Journal of Constructional Steel Research, 2024, 222: 108958.

[18] Li G Q, Jiang Y H, Zhong Y L, et al. Studies on resistance behavior of modified blind-bolts under pure tension and shear[J]. Journal of Constructional Steel Research, 2023, 210: 108114.

[19] You Y, Zhu H, Liu X, et al. Post fire tensile behavior of thread-fixed one-side bolt strengthened by backing plate[J]. Engineering Structures, 2022, 252: 113577.

[20] You Y, Liu M, Liu Y, et al. Experimental studies on thread-fixed one-side bolted T-stubs in tension at elevated temperatures[J]. Journal of Constructional Steel Research, 2020, 171: 106139.

[21] Wang P, You Y, Wang Q, et al. Post-fire tensile behavior of hole-anchored bolted T-stub connection[J]. Journal of Constructional Steel Research, 2021, 187: 106941.

[22] P398. Steel Construction Institute. Joints in Steel Construction: Moment-Resisting Joint to Eurocode 3 (2014)

[23] Wang W, Zhang Y, Xu L, et al. Mechanical properties of high-strength Q960 steel at elevated temperature[J]. Fire safety journal, 2020, 114: 103010.

[24] BS EN 1993-1-2. Design of Steel Structures - Part 1-2: General Rules - Structural Fire Design European Committee for Standardization, Brussels (2005)

[25] Pang X P, Hu Y, Tang S L, et al. Physical properties of high-strength bolt materials at elevated temperatures[J]. Results in Physics, 2019, 13: 102156.

[26] GB 50017–-2017. Code for Design of Steel Structure. China Architecture Publishing & Media Co. Ltd. Beijing (2017). (in Chinese)

[27] Wang F, Zhao O, Young B. Testing and numerical modelling of S960 ultra-high strength steel angle and channel section stub columns[J]. Engineering Structures, 2020, 204: 109902.

[28] Pijpers R J M, Slot H M. Friction coefficients for steel to steel contact surfaces in air and seawater[C]//Journal of Physics: Conference Series. IOP Publishing, 2020, 1669(1): 012002.

[29] Wang P, You Y, Xu Q, et al. Shear Behavior of Lapped Connections Bolted by thread-fixed one-side bolts at elevated temperatures[J]. Fire Safety Journal, 2021, 125: 103415.

[30] Yu H, Burgess I W, Davison J B, et al. Numerical simulation of bolted steel connections in fire using explicit dynamic analysis[J]. Journal of Constructional Steel Research, 2008, 64(5): 515-525.

[31] Wang P, You Y, Liu M, et al. Behavior of thread-fixed one-side bolted T-stubs with backing plates at ambient and elevated temperatures[J]. Journal of Constructional Steel Research, 2020, 170: 106093.

[32] You Y, Gu H, Wang Q, et al. Fire behavior of novel Thread-anchored One-side bolted connection with internal component[J]. Journal of Constructional Steel Research, 2022, 194: 107337.

[33] GB/T 192–-2003. National Standard of Peoples Republic of China, General Purpose Metric Screw Threads-basic Profile. China Construction Press (2003). (in Chinese)

[34] GB/T 196–-2003. National Standard of Peoples Republic of China, General Purpose Metric Screw Threads-basic Dimensions. China Construction Press (2003). (in Chinese)

[35] Liu Y, You Y, Bai Y, et al. Behavior of Square Hollow Section column connection using Thread-anchored One-side Bolt under tensile force at high temperature[J]. Journal of Building Engineering, 2022, 50: 104150.

[36] You Y, Le L, Xiao J, et al. A numerical investigation of the tensile behavior of the thread-fixed one-side bolted T-stubs at high temperature[J]. Steel and Composite Structures, 2022, 45(4): 605.

[37] Wang P, Sun L, Liu M, et al. Experimental studies on thread-fixed one-side bolted connection of beam to hollow square steel tube under static bending moment[J]. Engineering Structures, 2020, 214: 110655.